NIH Public Access
Author Manuscript
Eur J Neurosci. Author manuscript; available in PMC 2010 May 14.

Published in final edited form as:
Eur J Neurosci. 2009 December ; 30(12): 2271–2283. doi:10.1111/j.1460-9568.2009.07017.x.

BACE1 elevation in transgenic mouse models of Alzheimer's disease is associated with synaptic/axonal pathology and amyloidogenesis: Implication for neuritic plaque development

Xue-Mei Zhang[1,5,#], **Yan Cai**[2,3,#], **Kun Xiong**[3], **Huaibin Cai**[4], **Xue-Gang Luo**[3], **Jia-Chun Feng**[5], **Richard W. Clough**[1], **Robert G. Struble**[6], **Peter R. Patrylo**[1,2], and **Xiao-Xin Yan**[1,*]

[1]Department of Anatomy, Southern Illinois University School of Medicine, Carbondale, IL 62901, USA

[2]Department of Physiology, Southern Illinois University School of Medicine, Carbondale, IL 62901, USA

[3]Department of Anatomy and Neurobiology, Central South University Xiangya Medical School, Changsha, Hunan 410013, China

[4]Laboratory of Neurogenetics, National Institute on Aging, National Institutes of Health, Bethesda, MD 20892, USA

[5]Department of Neurology, The First Hospital of Jilin University, Changchun, Jilin 130021, China

[6]Center for Alzheimer's disease, Southern Illinois University School of Medicine, Springfield, IL 62794, USA

Abstract

Neuritic plaques are a pathological hallmark of Alzheimer's disease (AD). However, the origin of extracellular amyloid peptide (Aβ) deposits and the process of plaque development remain poorly understood. The present study attempted to explore plaque pathogenesis by localizing β-secretase-1 (BACE1) elevation relative to amyloid peptide (Aβ) accumulation and synaptic/neuritic alterations in the forebrain using transgenic (Tg) mice harboring familial AD (FAD) mutations (5XFAD and 2XFAD) as models. In animals with fully-developed plaque pathology, locally elevated BACE1 immunoreactivity (ir) coexisted with compact-like Aβ deposition, with BACE1-ir occurring selectively in dystrophic axons of various neuronal phenotypes or origins (GABAergic, glutamatergic, cholinergic or catecholaminergic). Prior to plaque onset, localized BACE1/Aβ-ir occurred at swollen presynaptic terminals and fine axonal processes. These BACE1/Aβ-containing axonal elements appeared to undergo a continuing process of sprouting/swelling and dystrophy, during which extracellular Aβ-ir emerged and accumulated in surrounding extracellular space. These data suggest that BACE1 elevation and associated Aβ overproduction inside the sprouting/dystrophic axonal terminals coincide with the onset and accumulation of extracellular amyloid deposition during the development of neuritic plaques in transgenic models of AD. Our findings appear in harmony with an early hypothesis that axonal pathogenesis plays a key or leading role in plaque formation.

Keywords

Aging; secretase; senile plaques; dystrophic neurite; axonopathy; neuroplasticity

*Correspondence to: Xiao-Xin Yan, Department of Anatomy, Southern Illinois University School of Medicine, Carbondale, IL 62901. Tel: 618-453-1577; xyan@siumed.edu .
[#]Authors contributed to this work equally.

NIH-PA Author Manuscript
NIH-PA Author Manuscript
NIH-PA Author Manuscript

NIH-PA Author Manuscript

NIH-PA Author Manuscript

NIH-PA Author Manuscript

Introduction

Neuritic plaques are localized lesions in the brain of Alzheimer disease (AD) composed of extracellular β-amyloid peptide (Aβ) deposits and dystrophic neurites. Amyloid accumulation is considered to play a central role in AD pathogenesis by causing synaptic damage, neuritic alteration, glial activation and neuronal death (Garcia-Alloza et al., 2006; Koenigsknecht-Talboo et al., 2008; Meyer-Luehmann et al., 2008; Koffie et al., 2009). However, the origin of Aβ deposits and the process of plaque formation in the brain remain largely unclear. Currently, extracellular Aβ deposits are proposed to derive from neuronal, glial and vascular components (Fiala, 2007). It is suggested that plaque formation may begin with small "nuclei" or "seeds" of insoluble Aβ fibrils, which develop into overt plaques through attracting available peptides in the area, governed by the fibrillaric nature of Aβ peptides (Ganowiak et al., 1994; Kane et al., 2000; Walker et al., 2002; Meyer-Luehmann et al., 2006; Eisele et al., 2009).

Historically, the site-specific plaque formation in the brain has been long thought perhaps a consequence of increased local amyloid production. In particular, the dystrophic neurites around the plaques were considered as the potential source of the locally-deposited amyloid substance (see reviews by Arendt et al., 2005; Gouras et al., 2005; Fiala, 2007). Neuritic or compact plaques can be divided into small primitive form and relatively large-sized, cored form, with the latter containing a central core of virtually pure or highly concentrated amyloid deposits (Fiala, 2007). Based on electron microscopic examination, Terry and Wisniewski (1970) proposed that primitive plaques may evolve into cored plaques as the amyloid materials accumulate inside the growing cluster of the dystrophic neurites.

The present study attempted to explore the origin and evolution of neuritic plaque by localizing β-secretase-1 (BACE1) elevation relative to Aβ accumulation and neuritic alteration in two transgenic (Tg) mouse models (5XFAD and 2XFAD mice) harboring familial AD (FAD) related mutations in amyloid precursor protein (APP) and presenilin-1 (PS1), based on the following rationales. (1) BACE1 initiates the amyloidogenic processing of APP; therefore, early or active amyloidogenic loci might exhibit site-specific BACE1 and Aβ elevation. (2) BACE1 protein and enzymatic activity are increased the brains of sporadic and familiar AD cases (Citron et al., 1992; Fukumoto et al., 2002; Holsinger et al., 2002; Yang et al., 2003), and in various transgenic models of AD (Citron et al., 1992; Rossner et al., 2001; Zhao et al., 2007); therefore, site-specific BACE1 elevation is expected to be detectable in the diseased brain. (3) Transgenic models of AD would be of particular value to allow an analysis of pathological evolution with age in comparable brain regions. The 5XFAD and 2XFAD transgenic mouse models have been well characterized (Borchelt et al., 1997; Oakley et al., 2006). These mice develop human-like neuritic plaques in the brain in an age-dependent manner, and they show cognitive deficits and synaptic dysfunction, which appear to be attributable to cerebral amyloid accumulation (Savonenko et al., 2005; Garcia-Alloza et al., 2006; Oakley et al., 2006; Yan et al., 2009).

Materials and Methods

Transgenic and non-transgenic mice

Male transgenic and non-transgenic mice were used in this study. Breeders of 2XFAD (APPswe, PSEN1dE9) (Borchelt et al., 1997) and 5XFAD (APPSwFlLon, PSEN1*M146L*L286V) (Oakley et al., 2006) mice, and adult BACE1 knockouts (B6.129-$Bace^{tm1Pcw}$/J, n=3) and wildtype littermates (n=3) (Cai et al., 2001) were purchased from the Jackson Laboratory (Bar Harbor, ME, USA), with a small colony of each transgenic strain maintained on-campus for the present study. 5XFAD mice undergo an aggressive course of plaque pathogenesis (Oakley et al., 2006), and they were examined at postnatal day 30–45

NIH-PA Author Manuscript

NIH-PA Author Manuscript

NIH-PA Author Manuscript

(n=6, with P0 referred to as the day of birth) and 2, 3, 4, 6 and 8 months (n=3–5 per age point for anatomical study and n=3 per age point for biochemical studies). 2XFAD mice undergo a less aggressive course of pathogenesis (Borchelt et al., 1997), and therefore were examined at 6 (n=4 for immunohistochemistry and n=3 western blot), 9 (n=4), 12 (n=4 for immunohistochemistry and n=3 western blot), 18 (n=3) months. C57BL/6L mice were offsprings of in-house breeders, and their brains were batch-processed with transgenic counterparts at matched age points with comparable sample size.

Animal use was in accordance with the National Institute of Health Guide for the Care and Use of Laboratory Animals. All procedures in the present study were approved by the Animal Care and Use Committee of Southern Illinois University.

Tissue preparation

For anatomical studies, animals were transcardially perfused with 4% paraformaldehyde in 0.01M phosphate-buffered saline (pH 7.4, PBS) following overdose anesthesia (sodium pentobarbital 100 mg/kg, i.p.). Brains were dissected out and postfixed overnight, and then cryoprotected in 30% sucrose at 4 °C. The two cerebral hemispheres of each brain were cut coronally and sagittally in a cryostat. For the purpose of batch-processing sections from a group of brains (at different ages), fiducial needle punches were made during cutting at different cortical locations for different brains, and these needle markers were used to identify sections from individual brains after an identical staining. A total of 12 sets of 30 μm-thick sections across the entire brain were collected consecutively in PBS in cell culture plates. In addition, 6 sets of 12 μm (processed free-floating) and 12 sets of 6 μm (thaw-mounted, immunostained on-slide) coronal sections were collected from the striatum to hippocampus levels, which were used to study colocalizations of various markers around the amyloid plaques and at fine neuronal terminals, respectively.

For biochemical studies, brains were briefly perfused with cold PBS to remove blood, and the cerebral cortex of one hemisphere was separated and snap-frozen with liquid nitrogen. Cortical samples from all age groups were stored at −70 °C, and batch-processed to assess BACE1 protein levels, enzymatic activity of β-site APP cleavage and soluble Aβ levels.

Immunohistochemistry

For immunolabeling with the peroxidase-DAB method, sections were treated with 1% H_2O_2 in PBS for 30 minutes, and pre-incubated in 5% normal goat or horse serum with 0.3% Triton X-100 for 1 hour. Antigen retrieval techniques were used for BACE1 (50% formamide and 50% 2XSSC at 65 °C for 1 hour) and Aβ antibody (50% formic acid in PBS for 30 minutes at room temperature) labelings before H_2O_2 treatment. Sections were incubated overnight at 4 °C with primary antibodies diluted in PBS containing appropriate blocking sera (see Table 1 for antibody sources and dilutions), reacted with biotinylated goat anti-rabbit, horse anti-mouse or rabbit anti-goat IgGs at 1:400 for 2 hours, and subsequently with the ABC reagents (1:400) (Vector Laboratories, Burlingame, CA, USA) for an additional hour. Immunoreactivity was visualized using 0.003% H_2O_2 and 0.05% diaminobenzidine (DAB, Sigma-Aldrich, St. Louis, MO, USA), with or without 0.025% NiCl and 0.025% CoCl enhancement.

Double immunofluorescence was carried out by incubating sections in PBS containing 5% donkey serum and a pair of primary antibodies from different animal species (Table 1), followed by a 2 hour reaction with Alexa Fluor® 488 and Alexa Fluor® 594 conjugated donkey anti-mouse, rabbit or goat IgGs (1:200, Invitrogen, Carlsbad, CA, USA). After fluorescent immunolabeling, sections were counter-stained with bisbenzimide (Hoechst 33342, 1:50000), washed 3 times in PBS and mounted with anti-fading medium. Initial antibody specificity tests

NIH-PA Author Manuscript

NIH-PA Author Manuscript

NIH-PA Author Manuscript

entailed preabsorption of primary antibody with neutralizing peptide and omission of primary antibody in the incubation buffer. These controls yielded no specific labeling in brain sections.

NADPH-diaphorase histochemistry

Sections (12 μm thick) were incubated in 0.05 M Tris-HCl buffered saline (pH 8.0, TBS) containing 0.3% Triton X-100, 1 mM nicotinamide adenine dinucleotide phosphate diaphorase (β -NADPH-d, N7505, Sigma-Aldrich), 0.8 mM nitroblue tetrazolium (NBT, N6639, Sigma-Aldrich) and 5% dimethyl sulfoxide for 45 and 15 minutes at 37 °C (Yan et al., 1996). The shorter incubation was used to yield a lighter NBT (blue) reactivity that would not mask DAB reaction products (brown) in double labeling preparation. Selected sections were further immunostained for other neuronal markers using the DAB-peroxidase method to assess colocalization.

Western blot

Cortical samples were homogenized by sonication in T-PER buffer (10x w/v) (Pierce, Rockford, IL, USA) containing a cocktail of protease inhibitors (Roche, Indianapolis, IN, USA), and centrifuged at 15,000 × *g* at 4 °C for 10 minutes. The supernatants were collected, and protein concentrations determined by DC protein assay (Bio-Rad Laboratories, Hercules, CA, USA). Twenty-five μg proteins were run on each lane in 12% SDS-PAGE gels (Hoefer Scientific Instruments, San Francisco, CA, USA). The polypeptides were electrotransferred to Trans-Blot® pure nitrocellulose membrane (Bio-Rad Laboratories). Nitrocellulose membranes were immunoblotted with anti-BACE1α (1:2000) and re-blotted for β-tubulin-III (rabbit antibody, T2200, 1:10000, Sigma-Aldrich, St. Louis, MO, USA), and signal was visualized with HRP-conjugated goat-anti-rabbit IgG (1:20000, Bio-Rad Laboratories) and the ECL Plus™ Western Blotting Detection kit (GE Healthcare Life Sci., Piscataway, NJ, USA). Immunoblot images were captured in a UVP Biodoc-it™ system (UVP, Inc, Upland, CA, USA).

Enzyme activity assay for β-site APP cleavage and ELISA for soluble Aβ concentration

A set of brain extracts from selected age groups was divided into two parts on the experimental day prior to a correlated analysis of putative BACE1-mediated activity of β-site APP cleavage and soluble Aβ levels in the same samples. β-Site APP cleavage activity was measured in 96-well transparent flat-bottom plates using a commercial kit (#565785, Calbiochem, La Jolla, CA, USA) following manufacturer's instruction. The signal was captured in a Bio-Rad microplate reader, and also imaged in the UVP Biodoc-it™ device. Levels of pan-Aβ species were assayed using a commercial kit according to manufacturer's instruction (Biosource International, Camarillo, CA, USA), except that the reporter antibody supplied by the manufacturer was replaced with biotinylated 4G8 diluted at 1:4000. Equal quantities (50 μg) of proteins were loaded in each well. The brain extracts were assayed in 3 experiments, with each analyzed a different set of brain extracts in duplicated loadings.

Imaging, data analysis, statistic testing

Sections were examined on an Olympus (BX60) fluorescent microscope equipped with a digital camera and image analysis system (Optronics, Goleta, CA, USA). A Zeiss fluorescent microscope (Axio Imager, equipped with Apo Tom analysis system, Germany) was used to study colocalization of immunolabelings at neuronal terminals in the 6 μm-thick sections, with fluorescence from the superficial ~4 μm tissue captured for image analyses. Images (1600×1200 pixels) were taken using 4X to 40X objective lens (with an ocular lens at 10X). A Nikon microscale standard was photographed accordingly for calibration purpose. Optic density in area of interest was measured with the OptiQuant analysis software (Parkard Instruments, Meriden, CT, USA), using the rectangular (for sampling western band signal) or

NIH-PA Author Manuscript

NIH-PA Author Manuscript

NIH-PA Author Manuscript

irregular interconnecting (for sampling section immunolabeling) tools. All imaging and biochemical data were exported into Excel spreadsheets. Specific signal was calculated according to the internal reference in a given assay, e.g., β-tubulin-III in western blot or peptide standard in ELISA. In the case of immunolabeling, optic densities obtained from comparable areas of identically-processed non-transgenic sections were used as cut-off threshold to define specific densities of corresponding labelings in transgenics. For the purpose of across-age comparison, data were normalized to appropriate age group of either the transgenics or the non-transgenic controls. Means were analyzed statistically using student-*t* test or one-way ANOVA with Bonferroni posttests (Prism GraphPad 4.1, San Diego, CA, USA). The minimal significance level was set at $p<0.05$. Figure panels were assembled using Photoshop 7.1.

Results

Localization of BACE1 immunoreactivity to neuronal terminals in non-transgenic brain

Anti-BACE1a was raised in rabbit with an immunogen corresponding to the N-terminal 46–163 amino acids of human BACE1 (Cai et al., 2001). In western blot this antibody recognizes mature BACE1 proteins migrating at ~70 kd as a relatively wide and somewhat fuzzy band in cell lysate and brain homogenate, and no specific signal is detectable in BACE1 knockout mouse brain extract (BACE1−/−) (Laird et al., 2005; Xiong et al., 2007; Yan et al., 2007; Wang et al., 2008). In immunohistochemistry, wildtype (BACE+/+) mouse brain sections exhibited region and lamina-specific immunoreactivity (ir), whereas no signal existed in identically-processed BACE1−/− brain sections (Fig. 1A).

The distribution pattern of BACE1-ir was essentially identical in the brains of BACE+/+ and C57BL/6L control mice at all ages examined in the present study. Overall, heavy BACE1-ir was present in the olfactory glomeruli and mossy fiber terminals, with weak, diffuse labeling occurring in the neuropil over most brain regions (Figs. 1A, B, E; 2C). Moderate non-cellular labeling appeared in the ventral pallidum and substantia nigra pars reticulata (Fig. 1A, C). Throughout the cortex, amygdala and hippocampal cellular layers, BACE1-ir was restricted to the neuropil (Figs. 1B, D).

Elevation of BACE1 protein, activity and Aβ levels with age in transgenic brain

Before comparative anatomical studies, we used anti-BACE1α to detect potential age-dependent elevation of cerebral BACE1 protein in transgenics relative to non-transgenic cohorts (Fig. 2A, B). Consistent with a previous report (Zhao et al., 2007), BACE1 protein levels in the cortex of 1 to 8 month-old 5XFAD mice were increased significantly relative to C57BL/6B mice, and the extent of change positively correlated with age (n=3/age, $p<0.0001$, $F=87$, $R^2=0.96$l one-way ANOVA test). Bonferroni's multiple comparison test showed statistically significant differences between individual 4–8 month-old 5XFAD groups and non-transgenic groups at 1, 6 or 12 month-old. Similarly, BACE1 protein levels in 2XFAD mouse cortex were increased at 12 relative to 6 month of age ($p=0.04$), but elevated relative to non-transgenics at 6 ($p=0.013$) and 12 ($p=0.001$) month (paired student-*t* tests) (Fig. 2B).

Cortical extracts from 5XFAD and C57BL/6L mice at 1–8 month of age were assayed to test if BACE1 enzymatic activity increased in transgenics with age in parallel with Aβ rise. β-Site APP cleavage activity in 5XFAD samples was significantly increased relative to non-transgenic controls, which correlated with age positively ($p<0.0001$, $F=59$, $R^2=0.95$, one-way ANOVA test, same below) (Fig. 2C, D). Similar age-related increase in soluble Aβ levels was detected in 5XFAD cerebrum by a sensitive ELISA targeting pan-Aβ species ($p<0.0001$, $F=75$, $R^2=0.93$), which was positively correlated with increased β-site APP cleavage activity in the same cortical samples ($p<0.002$, $r=0.91$) (Fig. 2D).

NIH-PA Author Manuscript

NIH-PA Author Manuscript

NIH-PA Author Manuscript

Occurrence of BACE1 immunoreactivity in dystrophic axons in transgenic brain

For anatomical studies, we first used anti-BACE1α to replicate previous finding of elevated BACE1-ir around amyloid plaques in 5XFAD and 2XFAD mice with established pathology (Zhao et al., 2007). Plaques were assessed with antibodies to pan-Aβ species (3D6, 4G8 and 6E10) and end-specific to Aβ40 (Ter-40) and Aβ42 (Ter-42) (Bard et al., 2000; Nishitsuji et al., 2007). These antibodies yielded largely comparable extracellular Aβ deposition patterns (data not shown). 3D6 and 6E10 were used as the primary Aβ antibodies in subsequent analyses as they exhibited novel difference regarding labelings around cerebral principal neurons, which appeared to be important for understanding antibody specificity. In brief, the pattern of 3D6-ir in 6–8 month-old 5XFAD and 9–18 month-old 2XFAD mice appeared to be optimal for compact amyloid plaques (as defined for instance by Fiala, 2007) in cortical and subcortical structures (Fig. 3D, L).

In contrast to identically processed C57BL/6L cohorts (Fig. 3A–C), localized heavy BACE1-ir was seen clearly in 5XFAD and 2XFAD forebrain. This selective BACE1 labeling colocalized with 3D6-ir around virtually all visible plaques at low magnification (Fig. 3E–G, M–O). At high magnification, BACE1-ir appeared to be associated with neuronal processes arranged in a rosette-like fashion, often with a grape-like swollen head at the periphery (Fig. 3H–K). In larger plaques, BACE1 labeled processes surrounded a central cavity occupied by dense Aβ-ir. In smaller plaques a central cavity was not visible, yet strongest Aβ-ir often existed at this location (Fig. 3H–K). Thus, BACE1/3D6 double labeling clearly displayed the so-called primitive and cored neuritic or compact plaques, namely plaques without and with, respectively, a central zone completely occupied by Aβ deposits (Fiala, 2007). It should be noted that weak 3D6-ir appeared to colocalize with BACE1-ir inside the swollen processes, which could be better appreciated by using a slightly longer exposure (Aβ-ir in the plaque core might become bleached in this case) (Fig. 3K).

Double immunofluorescence was used to clarify the axonal or dendritic (or both) nature of BACE1 labeled processes. These processes colocalized fully with synaptophysin (SYN), a marker of presynaptic axon terminals (Fig. 4A–D). BACE1 labeled processes also commonly co-expressed growth-associated protein-43 (GAP43), a marker of outgrowing/sprouting or highly plastic axon terminals (Fig. 4E–H). In contrast, BACE1-ir did not colocalize with microtubule associated protein-2 (MAP2), a marker for dendritic processes (Fig. 4I–L).

To verify BACE1-labeled axonal processes potentially being dystrophic neurites, we assessed coexistence of BACE1-ir with various markers that reportedly label dystrophic neurites. Similar colocalization patterns were observed in 5XFAD and 2XFAD mice. Briefly, BACE1-ir commonly colocalized with APP (Fig. 4M–O) and likely with presenilin-1 (PS1) (Fig. 4 P–R) in dystrophic-like neurites (Chui et al., 1998; Hendriks et al., 1998; Blanchard et al., 2003). In a given plaque, a subset of BACE1 labeled processes co-expressed one or another neuronal phenotype/transmitter marker reportedly labeling dystrophic neurites, including glutamic acid decarboxylase 67 (GAD67) (Fig. 5A–C), vesicular glutamate transporter-1 (VGLUT1) (Fig. 5D–F), choline acetyltransferase (ChAT) (Fig. 5G–I), tyrosine hydroxylase (TH) [Supplemental (S)-Fig. 1A, B], NADPH-d (Fig. 5J–L; S-Fig. 1C–F), or calbindin and parvalbumin (data not shown) (Struble et al., 1987; Walker et al., 1988; Quinn et al., 2001; Perez et al., 2007; Liu et al., 2008). In some cases, NADPH-d positive dystrophic neurites appeared to derive from axon-like processes of nitrinergic interneurons (Fig. 5K, L) (Yan et al., 1996). To understand as to why BACE1 colocalized partially with a given neuronal phenotype marker among dystrophic neurites, we also carried out double labelings for different combinations of neuronal markers. These experiments indicated that subsets of dystrophic neurites within the same plaque might actually express different neuronal markers, for instances, GAD65/67 vs VGLUT1 (Fig. 5M), ChAT vs VGLTU1 (Fig. 5N), VGLUT1 vs NADPH-d (Fig. 5O), and ChAT vs NADPH-d (Fig. 5P).

NIH-PA Author Manuscript

NIH-PA Author Manuscript

NIH-PA Author Manuscript

Besides the initial antibody specificity tests, authentic immunolabeling for a given antibody was vigorously cross-validated in the present study against its established characteristic positive and negative labeling pattern. For examples, no cell bodies were labeled by antibodies targeting neuronal terminals (SYN, GAP43, MAP2 and VGLUT1). SYN-ir was abundant in the hippocampal mossy fiber terminals (Fig. 4A), and heavy GAP43-ir occurred in the stratum lacunosum-moleculare and inner molecular layer (Fig. 4E). VGLUT1-ir was very intense in the olfactory glomeruli, the axon terminal field of the glutamatergic olfactory sensory neurons (not shown). The APP and PS1 antibodies labeled the somata of putative pyramidal neurons in addition to dystrophic neurites (Fig. 4N, Q), and the ChAT antibody also selectively detected large projective cholinergic neurons in the nucleus basalis of Meynert (Fig. 5H) and small cholinergic interneurons in the cerebral cortex (Fig. 5P). In all immunofluorescent studies, labeled dystrophic neurites were differentiated from cell bodies based on the fact that they were not associated with bisbenzimide nuclear labeling (e.g., Fig. 5M). Finally, there existed a clear consistency regarding colocalization or lack of colocalization between the tested markers in neuronal structures among various double-labeling preparations.

Early occurrence of BACE1/Aβ immunoreactivity at synaptic boutons in transgenic brain

Focal and punctuate BACE1 and 3D6 immunoreactive profiles were noticed in the forebrain during the study of transgenics with established plaque pathology (Figs. 3P, Q; 4I; 5A; S-Fig. 1C, D). To determine these profiles as potential "precursors" of overt plaques, we "back-tracked" BACE1 and Aβ antibody (shown are 3D6 and 6E10) labelings to the ages prior to or in the early stage of plaque onset in 5XFAD (S-Figs. 2, 3) and 2XFAD (not shown) mice. Overall, there existed a spatiotemporal overlap between BACE1 and Aβ antibody labelings around cortical and hippocampal neurons and plaques. In brief, 3D6, 6E10 and BACE1 immunolabelings were detectable in 5XFAD mice as early as 1 month of age selectively around a subset of pyramidal neurons in cortical layer V, subiculum and hippocampal CA1 (S-Fig. 2). These labelings appeared to spread to and increase numerically across the cortical layers and along the anterioposterior cerebral dimension during the following months (S-Fig. 3). Interestingly, a rostrocaudal progression pattern was seen in cerebral sagittal sections from 1 to 8 month of age, which was in parallel between BACE1 and Aβ antibody labelings (S-Figs. 2A, C, E; 3A, B, G–J).

However, the most novel findings in these developmental studies were the differential 3D6/BACE1 labelings relative to 6E10 around cortical and hippocampal pyramidal neurons, and the occurrence of the aforementioned focal and punctuate BACE1/3D6 labeling before plague onset. Thus, in 1 month-old pre-plaque 5XFAD mice, punctuate or granule-like 3D6-ir occurred around layer V pyramidal neurons mostly arranged along but sometimes protruding beyond the cell boundary (S-Fig. 2A, B, G), whereas 6E10-ir appeared to be intrasomatic or cytoplasmic in these pyramidal neurons (S-Figs. 2C, D, H). Similar to, but not as distinct as 3D6, BACE1-ir appeared to be largely juxtamembranous rather than cytoplasmic around principal neurons (S-Figs. 2E, F, L). Around the time of plaque onset (1.5 to 2 month), the above-mentioned perisomatic (3D6, BACE1) and intrasomatic (6E10) labelings co-existed with small plaque-like profiles located discretely in cortical V at perisomatic locations (Fig. 6A, B; S-Fig. 3C–F), and with more prevalent plaque-like extracellular Aβ deposition in the subiculum (Fig. 6C, D).

As with the DAB-peroxidase preparations, BACE1 and 3D6 labeled elements in double immunofluorescence selectively occurred around a subset of layer V pyramidal neurons in 1 month-old 5XFAD mice (Fig. 6E–G), appearing granule-like at high magnification (Fig. 6G1). The amount, size and reactivity of these perisomatic elements appeared to increase with age thereafter. Thus, they tended to aggregate and expand to become small but distinct perisomatic "mini-plaques" (i.e., isolated swollen terminals surrounded by a small amount of extracellular

NIH-PA Author Manuscript

NIH-PA Author Manuscript

NIH-PA Author Manuscript

Aβ-ir) (Fig. 6A, B). In 2–6 month-old 5XFAD mouse cortex 3D6/BACE1 labeled perisomatic elements and mini-plaques coexisted with increasingly prevalent more-established compact plaques in a local area (Fig. 6H–J). As aforementioned, small BACE1/3D6 immunoreactive perisomatic profiles, with some appearing as mini-plaques, coexisted with larger and distinct neuritic plaques in the cortex in 2XFAD mice at various ages (Fig. 3P, Q).

BACE1/3D6 immunoreactive perisomatic elements colocalized with synaptophysin as cross-validated with two different (mouse and rabbit) antibodies, implicating these profiles being presynaptic terminals (Fig. 6K–P). We also found partial colocalization of BACE1-ir or 3D6-ir with VGLUT1 or GAD67/GAD65/67 around the perisomatic locations (data not shown). Moreover, BACE1 and Aβ labelings might overlap with fine NADPH-d plexuses, seemingly at axonal varicosities in some cases, before and after plaque onset (Fig. 6Q–Q2; S-Fig. 1E, F).

It should be clarified that although we described the perisomatic BACE1 and 3D6 terminal labelings in the cortex in great detail (since they were microscopically prominent), localized BACE1/3D6-ir was also detectable at axonal plexuses or isolated small swollen terminals in the cortex away from neuronal somata and plaques. In fact, the latter type of terminal labelings was predominant in brain areas/lamina without perikarya-associated Aβ antibody labelings, including cortical layer I and white matter (Figs. 3M, N; 5I; 6C, D; S-Fig. 1B, D, H), hippocampal non-cellular layers (Fig. 4E, I) and many subcortical areas such as the striatum (S-Fig. 1A, B, F).

Quantitative analysis of BACE1 and Aβ immunoreactivity relative to neuritic cluster size

A correlated densitometry was designated to profile the relationship or dynamics of BACE1/Aβ-ir with plaque-associated and pre-plaque dystrophic axons at selected ages. Coronal sections at the septal levels from transgenics and controls of the same age were batch-processed for BACE1 and 3D6 immunofluorescence. Images were taken with the 40X objective over the dorsal cortical regions (layers III-VI) using the same exposure settings for all sections. Individual clusters of BACE1 labeled swollen/dystrophic neurites were sampled by tracing along the most protruding points or outer skirts of the labeled processes using the irregular interconnecting tool (Fig. 7A). The measuring template created in BACE1 immunofluorescent image was copied and aligned coordinately over the 3D6 image of the same microscopic field. The areal sizes of, and BACE1-ir and 3D6-ir associated with, individual neuritic clusters were obtained. Immunoreactivities over comparable cortical regions in the nontransgenic sections were also measured, and used as cut-off threshold to calculate specific BACE1/Aβ reactivity in the transgenics (Fig. 7A–C).

Based on an analysis of ~500 individual profiles in 6 month-old 5XFAD mice, BACE1-ir appeared relatively stable from small to larger neuritic clusters. A trend of decline in BACE1-ir was noticeable among clusters approximately >1000 μm^2 (Fig. 7C1, C3). Overall, 3D6 reactivity appeared to increase in parallel with the enlargement of neuritic clusters, although this change was mostly evident among clusters between 50–1000 μm^2. 3D6-ir tended to maintain at a plateau of high reactivity among clusters approximately >1000 μm^2 (Fig. 7C1, C2).

Additional trials of the above correlated densitometry were carried out in sections from two other age groups of 5XFAD mice (2 and 4 month-old) as well as from the 12 month-old 2XFAD mouse group. Overall, data from these animals indicated that BACE1/3D6-ir exhibited similar patterns of variation relative to the change of neuritic cluster size (S-Fig. 4), as with the 6 month-old 5XFAD transgenics.

NIH-PA Author Manuscript

NIH-PA Author Manuscript

NIH-PA Author Manuscript

Discussion

BACE1 elevation in transgenic models of AD is largely localized to axonal structures

BACE1 enzymatic activity is obligatory in the amyloidogenic processing of APP. Hypothetically, BACE1 elevation might occur site-specifically in the brain, mediate local Aβ overproduction, and eventually lead to site-specific amyloid accumulation and plaque formation. The present study shows elevated BACE1 protein levels and activity in 5XFAD and 2XFAD mouse cortex in an age-dependent manner, consistent with previous reports in transgenic models of AD (Citron et al., 1992; Zhao et al., 2007). Putative BACE1-mediated β-site APP cleavage activity is increased in transgenic brain extracts with age, which appears to correlate with elevated soluble Aβ levels. Therefore, BACE1 elevation in the transgenic brain appears to be functionally relevant to Aβ rise.

Our immunohistochemical studies reveal distinct and localized BACE1-ir in 5XFAD and 2XFAD mouse forebrain in an age, region/lamina and neuronal element dependent manner. In contrast, BACE1-ir in nontransgenic mice appears weak and diffuse across the neuropil in most parts of the brain except for the olfactory bulb and hippocampus wherein BACE1-ir is heavily expressed at olfactory nerve and mossy fiber terminals (Yan et al., 2007). The increased BACE1-ir in transgenics is almost invariably associated with Aβ-ir visualized by 3D6, which clearly identifies extracellular Aβ deposits. Of note, little 3D6-ir occurs in neuronal cytoplasm wherein murine and/or human transgenic APP-ir is present (Blanchard et al., 2003; Zhao et al., 2007; and this study). Therefore, potential interpretive confusion between 3D6 identified Aβ being APP cross-reactivity appears to be minimal. Together with the biochemical data, the selective co-occurrence of BACE1 and 3D6-ir in neuronal elements is almost certainly representative of pathologically important amyloidogenic loci in vivo.

The term "neuritic dystrophy" may apply to both dendritic and axonal changes. It is important to note that plaque-related dendritic "dystrophy" appears as spine loss, curvature distortion and shrinkage of shaft diameter (Spires et al., 2005; Meyer-Luehmann et al., 2008; Knafo et al., 2009), whereas axonal dystrophy is characterized by grape-like swelling and rosette-like sprouting (Fiala et al., 2007). Based on morphological profiles, it appears that BACE1 elevation around compact plaques occurs selectively in dystrophic axons in 5XFAD and 2XFAD mouse forebrain. The double labeling data of the present study strongly support this conclusion. In particular, BACE1-ir in dystrophic neurites colocalizes with common axonal (SYN, GAP-43) but not dendritic (MAP-2) markers. Also, BACE1-ir occurs coincident with two other Aβ-producing proteins (APP and PS1) and Aβ per se in dystrophic neurites, and partially with one or another neurotransmitter marker.

Distinct and selective BACE1/3D6 labeling is detected at perisomatic synaptic boutons and axon varicosities before the appearance of the first wave of extracellular plaques (also during the course of follow-up plaque formation). As with the dystrophic neurites (Walker et al., 1988), this early axon terminal labeling appears to be a multisystem phenomenon, involving likely both glutamatergic and GABAergic terminals. These data suggest that BACE1 may mediate Aβ overproduction predominantly in axonal structures from multiple neuronal phenotypes in transgenic models of AD, and that the process appears to begin prior to overt extracellular amyloid deposition and proceeds throughout the course of plaque development.

Axonal amyloidogenesis may play a key role in neuritic plaque development

The origin of extracellular Aβ deposits and their temporal relationship with local neuritic pathology remain an ongoing debative issue in AD research. Plaque-associated neuritic (axonal and dendritic) dystrophy is commonly described as a subsequent event of amyloid deposition. However, it has been also proposed that neuritic changes perhaps precede Aβ deposition, as

NIH-PA Author Manuscript

NIH-PA Author Manuscript

NIH-PA Author Manuscript

mentioned in the introduction (Arendt et al., 2005; Gouras et al., 2005; Fiala, 2007). Recent evidence suggests that Aβ may be generated in and released by axon terminals, and be deposited as plaques at the axonal target sites (Lazarov et al., 2002; Sheng et al., 2002, 2003). In addition, axonal pathology may occur prior to amyloid deposition (Stokin et al., 2005).

In the present study, plaque-associated as well as pre-plaque dystrophic axons express the full set of amyloidogenic machinery and the end product (Aβ). When comparing small to larger plaques, weak Aβ-ir persists inside the dystrophic axons, whereas more substantial Aβ-ir accumulates around dystrophic axons as plaque size increases. This implicates extracellular Aβ deposition around dystrophic neurites potentially a paracrine-like phenomenon. Our densitometric analyses correlate 3 variables, areal size of the neuritic clusters, and BACE-ir and Aβ-ir associated with these individual clusters. The analysis is based on immunoreactivities in the same microscopic field (eliminating essentially all experimental and individual biases), and would reflect the true statuses between these variables among labeled profiles at the time of brain fixation. Data indicate that Aβ-ir accumulates locally as the neuritic clusters increase in size. Of note, Aβ-ir appears to increase rapidly during the initial phase of expansion of the neuritic clusters, and slow down afterwards. The latter trend could potentially relate to a centroperipheral shift of the dystrophic neurites in cored plaques that allows or brings about new space for amyloid deposition. The noticeable decline of BACE1-ir among larger clusters probably also relates to the enlargement of the amyloid core, which is included in the sampling area for the measurement of neuritic cluster size. Overall, our quantitative data appear in accordance with a recent in vivo time-lapsing study demonstrating a more rapid growth of smaller relative to larger plaques, which can be attenuated by blocking Aβ genesis with γ-secretase inhibitor (Yan et al., 2009).

Consistent with the above notion, we observe early BACE1/Aβ elevation at synaptic boutons or fine axon processes that are not associated with clear local extracellular (or extra-axonal) Aβ deposition. Some of these fine terminals appear to expand/sprout to become small neuritic clusters surrounded by a small amount of extracellular Aβ, forming mini-plaques. These early profiles seemingly further evolve into primitive plaques followed by maturation into cored plaques (Terry and Wisniewski, 1970). Together, the formation of neuritic plaques could be potentially viewed as a continuing process of synaptic/axonal pathology inherent with intra-axonal Aβ overproduction and local extracellular accumulation/deposition (Fig. 7D).

In summary, the present study elaborates the potential origin and evolution of neuritic plaques by correlating elevated BACE1 protein and activity with Aβ rise, and by localizing increased BACE1 reactivity relative to Aβ deposition and neuritic pathology in two transgenic models of AD. Increased BACE1 and Aβ labelings occur in axon terminals and axonal neurites of multiple neuronal phenotypes during plaque development, implicating axons as an important source for extracellular amyloid deposits. This notion is also supported by densitometric data that indicate increasing local Aβ deposition around growing dystrophic neuritic clusters.

Supplementary Material

Refer to Web version on PubMed Central for supplementary material.

Acknowledgments

This study was supported by Illinois Department of Public Health (X.X.Y.). We thank Elan, Drs. H. Mori and S. Gandy for providing antibodies.

NIH-PA Author Manuscript

NIH-PA Author Manuscript

NIH-PA Author Manuscript

References

Arendt T. Alzheimer's disease as a disorder of dynamic brain self-organization. Prog Brain Res 2005;147:355–378. [PubMed: 15581717]

Bard F, Cannon C, Barbour R, Burke RL, Games D, Grajeda H, Guido T, Hu K, Huang J, Johnson-Wood K, Khan K, Kholodenko D, Lee M, Lieberburg I, Motter R, Nguyen M, Soriano F, Vasquez N, Weiss K, Welch B, Seubert P, Schenk D, Yednock T. Peripherally administered antibodies against amyloid beta-peptide enter the central nervous system and reduce pathology in a mouse model of Alzheimer disease. Nat. Med 2000;6:916–919. [PubMed: 10932230]

Blanchard V, Moussaoui S, Czech C, Touchet N, Bonici B, Planche M, Canton T, Jedidi I, Gohin M, Wirths O, Bayer TA, Langui D, Duyckaerts C, Tremp G, Pradier L. Time sequence of maturation of dystrophic neurites associated with Abeta deposits in APP/PS1 transgenic mice. Exp. Neurol 2003;184:247–263. [PubMed: 14637096]

Borchelt DR, Ratovitski T, van Lare J, Lee MK, Gonzales V, Jenkins NA, Copeland NG, Price DL, Sisodia SS. Accelerated amyloid deposition in the brains of transgenic mice coexpressing mutant presenilin 1 and amyloid precursor proteins. Neuron 1997;19:939–945. [PubMed: 9354339]

Cai H, Wang Y, McCarthy D, Wen H, Borchelt DR, Price DL, Wong PC. BACE1 is the major beta-secretase for generation of Abeta peptides by neurons. Nat. Neurosci 2001;4:233–234. [PubMed: 11224536]

Chui DH, Shirotani K, Tanahashi H, Akiyama H, Ozawa K, Kunishita T, Takahashi K, Makifuchi T, Tabira T. Both N-terminal and C-terminal fragments of presenilin 1 colocalize with neurofibrillary tangles in neurons and dystrophic neurites of senile plaques in Alzheimer's disease. J. Neurosci. Res 1998;53:99–106. [PubMed: 9670996]

Citron M, Oltersdorf T, Haas C. Mutation of the β-Amyloid precursor protein in familial Alzheimer’s disease increases β-protein production. Nature 1992;360:672–674. [PubMed: 1465129]

Eisele YS, Bolmont T, Heikenwalder M, Langer F, Jacobson LH, Yan ZX, Roth K, Aguzzi A, Staufenbiel M, Walker LC, Jucker M. Induction of cerebral beta-amyloidosis: intracerebral versus systemic Abeta inoculation. Proc. Natl. Acad. Sci.U.S.A 2009;106:12926–12931. [PubMed: 19622727]

Fiala JC. Mechanisms of amyloid plaque pathogenesis. Acta. Neuropathol 2007;114:551–571. [PubMed: 17805553]

Fukumoto H, Cheung BS, Hyman BT, Irizarry MC. Beta-secretase protein and activity are increased in the neocortex in Alzheimer disease. Arch. Neurol 2002;59:1381–1389. [PubMed: 12223024]

Fukumoto H, Cheung BS, Hyman BT, Irizarry MC. Beta-secretase protein and activity are increased in the neocortex in Alzheimer disease. Arch. Neurol 2002;59:1381–1389. [PubMed: 12223024]

Ganowiak K, Hultman P, Engström U, Gustavsson A, Westermark P. Fibrils from synthetic amyloid-related peptides enhance development of experimental AA-amyloidosis in mice. Biochem. Biophys. Res. Commun 1994;199:306–312. [PubMed: 8123028]

Garcia-Alloza M, Robbins EM, Zhang-Nunes SX, Purcell SM, Betensky RA, Raju S, Prada C, Greenberg SM, Bacskai BJ, Frosch MP. Characterization of amyloid deposition in the APPswe/PS1dE9 mouse model of Alzheimer disease. Neurobiol. Dis 2006;24:516–524. [PubMed: 17029828]

Gouras GK, Almeida CG, Takahashi RH. Intraneuronal Abeta accumulation and origin of plaques in Alzheimer's disease. Neurobiol. Aging 2005;26:1235–1244. [PubMed: 16023263]

Hendriks L, De Jonghe C, Lübke U, Woodrow S, Vanderhoeven I, Boons J, Cras P, Martin JJ, Van Broeckhoven C. Immunoreactivity of presenilin-1 and tau in Alzheimer's disease brain. Exp. Neurol 1998;149:341–348. [PubMed: 9500965]

Holsinger RM, McLean CA, Beyreuther K, Masters CL, Evin G. Increased expression of the amyloid precursor beta-secretase in Alzheimer's disease. Ann. Neurol 2002;51:783–786. [PubMed: 12112088]

Kane MD, Lipinski WJ, Callahan MJ, Bian F, Durham RA, Schwarz RD, Roher AE, Walker LC. Evidence for seeding of beta -amyloid by intracerebral infusion of Alzheimer brain extracts in beta -amyloid precursor protein-transgenic mice. J. Neurosci 2000;20:3606–3611. [PubMed: 10804202]

Knafo S, Alonso-Nanclares L, Gonzalez-Soriano J, Merino-Serrais P, Fernaud-Espinosa I, Ferrer I, DeFelipe J. Widespread changes in dendritic spines in a model of Alzheimer's disease. Cereb Cortex 2009;19:586–592. [PubMed: 18632740]

NIH-PA Author Manuscript

NIH-PA Author Manuscript

NIH-PA Author Manuscript

Koenigsknecht-Talboo J, Meyer-Luehmann M, Parsadanian M, Garcia-Alloza M, Finn MB, Hyman BT, Bacskai BJ, Holtzman DM. Rapid microglial response around amyloid pathology after systemic anti-Abeta antibody administration in PDAPP mice. J. Neurosci 2008;28:14156–14164. [PubMed: 19109498]

Koffie RM, Meyer-Luehmann M, Hashimoto T, Adams KW, Mielke ML, Garcia-Alloza M, Micheva KD, Smith SJ, Kim ML, Lee VM, Hyman BT, Spires-Jones TL. Oligomeric amyloid beta associates with postsynaptic densities and correlates with excitatory synapse loss near senile plaques. Proc. Natl. Acad. Sci. U.S.A 2009;106:4012–4017. [PubMed: 19228947]

Laird FM, Cai H, Savonenko AV, Farah MH, He K, Melnikova T, Wen H, Chiang HC, Xu G, Koliatsos VE, Borchelt DR, Price DL, Lee HK, Wong PC. BACE1, a major determinant of selective vulnerability of the brain to amyloid-beta amyloidogenesis, is essential for cognitive, emotional, and synaptic functions. J. Neurosci 2005;25:11693–11709. [PubMed: 16354928]

Lazarov O, Lee M, Peterson DA, Sisodia SS. Evidence that synaptically released beta-amyloid accumulates as extracellular deposits in the hippocampus of transgenic mice. J. Neurosci 2002;22:9785–9793. [PubMed: 12427834]

Liu Y, Yoo MJ, Savonenko A, Stirling W, Price DL, Borchelt DR, Mamounas L, Lyons WE, Blue ME, Lee MK. Amyloid pathology is associated with progressive monoaminergic neurodegeneration in a transgenic mouse model of Alzheimer's disease. J. Neurosci 2008;28:13805–13814. [PubMed: 19091971]

Meyer-Luehmann M, Coomaraswamy J, Bolmont T, Kaeser S, Schaefer C, Kilger E, Neuenschwander A, Abramowski D, Frey P, Jaton AL, Vigouret JM, Paganetti P, Walsh DM, Mathews PM, Ghiso J, Staufenbiel M, Walker LC, Jucker M. Exogenous induction of cerebral beta-amyloidogenesis is governed by agent and host. Science 2006;313:1781–1784. [PubMed: 16990547]

Meyer-Luehmann M, Spires-Jones TL, Prada C, Garcia-Alloza M, de Calignon A, Rozkalne A, Koenigsknecht-Talboo J, Holtzman DM, Bacskai BJ, Hyman BT. Rapid appearance and local toxicity of amyloid-beta plaques in a mouse model of Alzheimer's disease. Nature 2008;451:720–724. [PubMed: 18256671]

Nishitsuji K, Tomiyama T, Ishibashi K, Kametani F, Ozawa K, Okada R, Maat-Schieman ML, Roos RAC, Iwai K, Mori H. Cerebral vascular accumulation of Dutch-type Ab42, but not wild-type Ab42, in hereditary cerebral hemorrhage with amyloidosis, Dutch type. J. Neurosci. Res 2007;85:2917–2923. [PubMed: 17628026]

Oakley H, Cole SL, Logan S, Maus E, Shao P, Craft J, Guillozet-Bongaarts A, Ohno M, Disterhoft J, Van Eldik L, Berry R, Vassar R. Intraneuronal β-amyloid aggregates, neurodegeneration, and neuron loss in transgenic mice with five familial Alzheimer’s disease mutations: potential factors in amyloid plaque formation. J. Neurosci 2006;26:10129–10140. [PubMed: 17021169]

Perez SE, Dar S, Ikonomovic MD, DeKosky ST, Mufson EJ. Cholinergic forebrain degeneration in the APPswe/PS1DeltaE9 transgenic mouse. Neurobiol. Dis 2007;28:3–15. [PubMed: 17662610]

Quinn J, Davis F, Woodward WR, Eckenstein F. Beta-amyloid plaques induce neuritic dystrophy of nitric oxide-producing neurons in a transgenic mouse model of Alzheimer's disease. Exp. Neurol 2001;168:203–212. [PubMed: 11259108]

Rossner S, Apelt J, Schliebs R, Perez-Polo JR, Bigl V. Neuronal and glial beta-secretase (BACE) protein expression in transgenic Tg2576 mice with amyloid plaque pathology. J. Neurosci. Res 2001;64:437–446. [PubMed: 11391698]

Savonenko A, Xu GM, Melnikova T, Morton JL, Gonzales V, Wong MP, Price DL, Tang F, Markowska AL, Borchelt DR. Episodic-like memory deficits in the APPswe/PS1dE9 mouse model of Alzheimer's disease: relationships to beta-amyloid deposition and neurotransmitter abnormalities. Neurobiol. Dis 2005;18:602–617. [PubMed: 15755686]

Sheng JG, Price DL, Koliatsos VE. Disruption of corticocortical connections ameliorates amyloid burden in terminal fields in a transgenic model of Aβ amyloidosis. J. Neurosci 2002;22:9794–9799. [PubMed: 12427835]

Sheng JG, Price DL, Koliatsos VE. The beta-amyloid-related proteins presenilin 1 and BACE1 are axonally transported to nerve terminals in the brain. Exp. Neurol 2003;184:1053–1057. [PubMed: 14769400]

Spires TL, Meyer-Luehmann M, Stern EA, McLean PJ, Skoch J, Nguyen PT, Bacskai BJ, Hyman BT. Dendritic spine abnormalities in amyloid precursor protein transgenic mice demonstrated by gene

NIH-PA Author Manuscript

NIH-PA Author Manuscript

NIH-PA Author Manuscript

transfer and intravital multiphoton microscopy. J. Neurosci 2005;25:7278–7287. [PubMed: 16079410]

Stokin GB, Lillo C, Falzone TL, Brusch RG, Rockenstein E, Mount SL, Raman R, Davies P, Masliah E, Williams DS, Goldstein LS. Axonopathy and transport deficits early in the pathogenesis of Alzheimer's disease. Science 2005;307:1282–1288. [PubMed: 15731448]

Struble RG, Powers RE, Casanova MF, Kitt CA, Brown EC, Price DL. Neuropeptidergic systems in plaques of Alzheimer's disease. J. Neuropathol. Exp. Neurol 1987;46:567–584. [PubMed: 2442313]

Terry, RD.; Wisniewski, HM. The ultrastructure of the neurobrillary tangle and the senile plaque. In: GEW, Wolstenholme; O'Connor, M., editors. Alzheimer's disease and related conditions. London: J & A Churchill; 1970. p. 145-168.

Walker LC, Bian F, Callahan MJ, Lipinski WJ, Durham RA, LeVine H. Modeling Alzheimer's disease and other proteopathies in vivo: is seeding the key? Amino Acids 2002;23:87–93. [PubMed: 12373522]

Walker LC, Kitt CA, Cork LC, Struble RG, Dellovade TL, Price DL. Multiple transmitter systems contribute neurites to individual senile plaques. J. Neuropathol Exp. Neurol 1988;47:138–144. [PubMed: 2828554]

Wang L, Shim H, Xie C, Cai H. Activation of protein kinase C modulates BACE1-mediated beta-secretase activity. Neurobiol. Aging 2008;29:357–367. [PubMed: 17157415]

Xiong K, Cai H, Luo XG, Struble RG, Clough RW, Yan XX. Mitochondrial respiratory inhibition and oxidative stress elevate beta-secretase (BACE1) proteins and activity in vivo in the rat retina. Exp. Brain Res 2007;181 435-346.

Yan P, Bero AW, Cirrito JR, Xiao Q, Hu X, Wang Y, Gonzales E, Holtzman DM, Lee JM. Characterizing the appearance and growth of amyloid plaques in APP/PS1 mice. J. Neurosci 2009;29:10706–10714. [PubMed: 19710322]

Yan XX, Jen LS, Garey LJ. NADPH-diaphorase-positive neurons in primate cerebral cortex colocalize with GABA and calcium-binding proteins. Cereb. Cortex 1996;6:524–529. [PubMed: 8670678]

Yan XX, Xiong K, Luo XG, Struble RG, Clough RW. Beta-Secretase expression in normal and functionally deprived rat olfactory bulbs: inverse correlation with oxidative metabolic activity. J. Comp. Neurol 2007;501:52–69. [PubMed: 17206602]

Yang LB, Lindholm K, Yan R, Citron M, Xia W, Yang XL, Beach T, Sue L, Wong P, Price D, Li R, Shen Y. Elevated beta-secretase expression and enzymatic activity detected in sporadic Alzheimer disease. Nat. Med 2003;9:3–4. [PubMed: 12514700]

Zhao J, Fu Y, Yasvoina M, Shao P, Hitt B, O'Connor T, Logan S, Maus E, Citron M, Berry R, Binder L, Vassar R. Beta-site amyloid precursor protein cleaving enzyme 1 levels become elevated in neurons around amyloid plaques: implications for Alzheimer's disease pathogenesis. J. Neurosci 2007;27:3639–3649. [PubMed: 17409228]

NIH-PA Author Manuscript
NIH-PA Author Manuscript
NIH-PA Author Manuscript

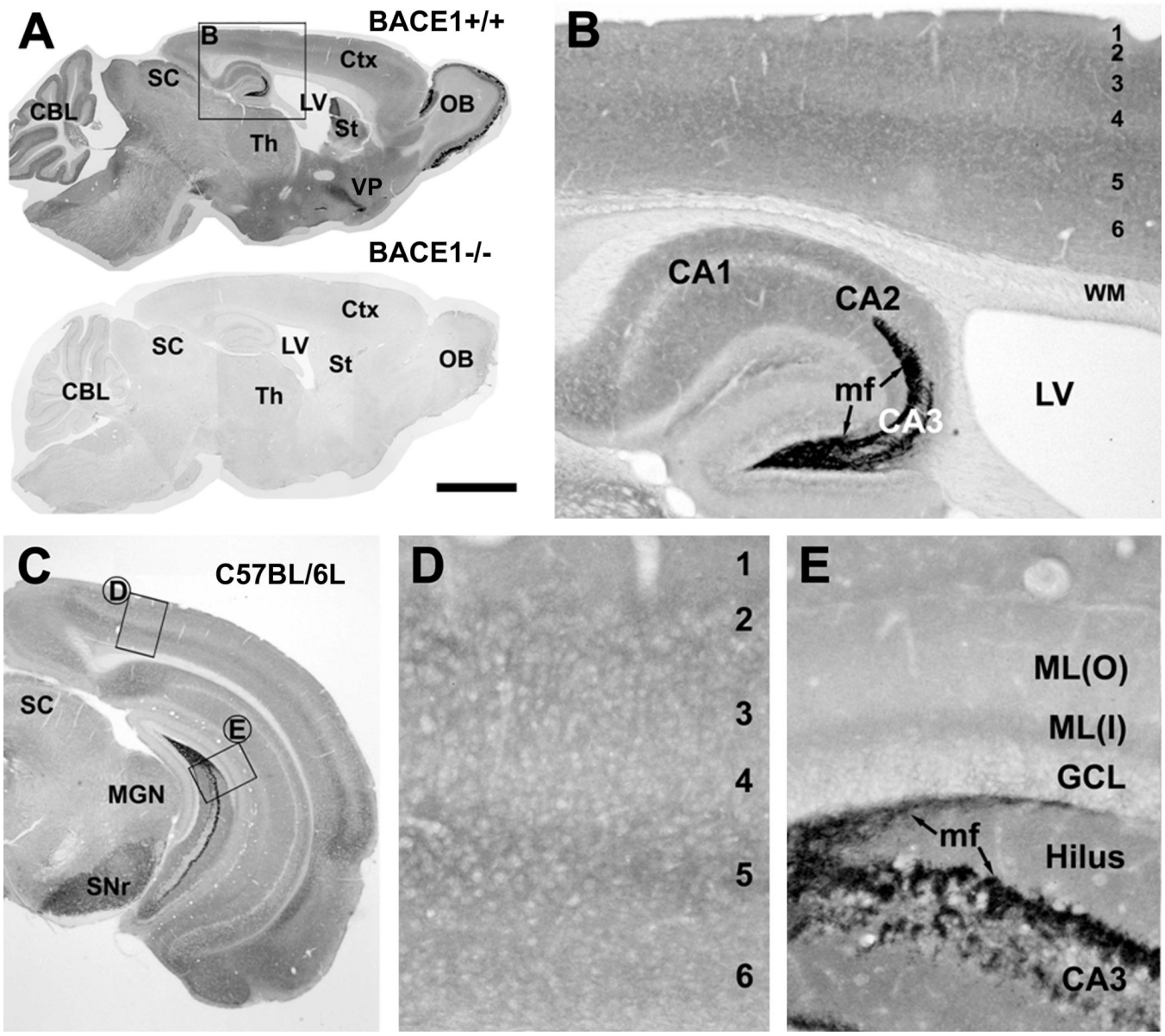

Fig. 1.

Immunohistochemical characterization of BACE1 in non-transgenic mouse brain using rabbit anti-BACE1α. Panel A shows selective BACE1 labeling in wild-type (BACE1+/+, top) but no signal in knockout (BACE1−/−, bottom) mouse brains following a batch processing of sagittal sections. The boxed area in A is enlarged as panel B. Panel C illustrates BACE1 labeling in a coronal section at the level of medial geniculate nucleus (MGN) from a 6 month-old C57BL/6L mouse, with two boxed areas enlarged as D and E. Note heavy BACE1 labeling in the olfactory bulb (OB) glomeruli (A) and hippocampal mossy fiber (mf) terminals (B, E). Diffuse and weak neuropil reactivity is present in the cortex (Ctx), amygdala and the remaining hippocampal areas (rather than mossy fiber terminals). Arab numbers indicate cortical layers. CBL: cerebellum, LV: lateral ventricle, St: striatum, Th: thalamus, VP: ventral pallidum, SC: superior colliculus, SNr: substantia nigra pars reticulata, WM: white matter, CA1-3: CA sectors of hippocampus, GCL: granule cell layer, ML(o) outer molecular layer, ML(i) inner molecular layer. Scale bar=2 mm in A, equal to 1 mm in C, 250 μm in B and 100 μm in D and E.

NIH-PA Author Manuscript
NIH-PA Author Manuscript
NIH-PA Author Manuscript

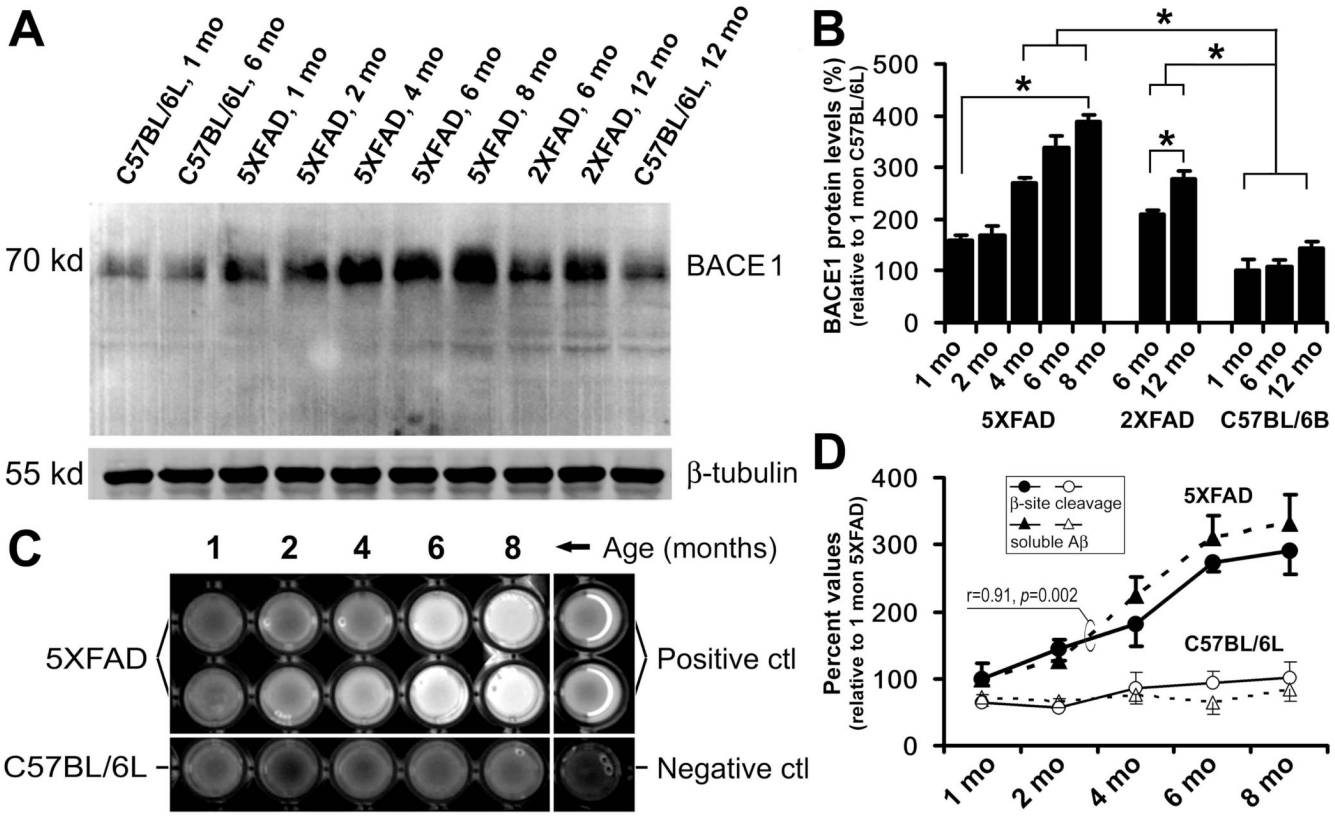

Fig. 2.

Biochemical analyses of age-related elevation of BACE1 protein levels (A, B), enzymatic activity of β-site amyloid precursor protein (APP) cleavage (C, D) and soluble Aβ levels (D). Values are expressed as mean±S.D. (%) normalized to indicated animal groups. Panel A shows a representative western analysis of cortical lysates from 5XFAD, 2XFAD and C57BL/6L control mice at indicated age points. BACE1 levels appear to increase with age in the transgenics relative to non-transgenic cohorts. Panel B summarizes data from three separate assays illustrating statistically significant (*) elevation of BACE1 protein levels in transgenics with age, and relative to non-transgenics. Panel C shows an example of BACE1 enzyme activity assay, illustrating increased fluorescent signals with age in 5XFAD samples relative to controls. Positive and negative assay controls are defined by incubations using company-supplied standard BACE1 enzyme and BACE1 inhibitor, respectively. Levels of soluble pan-Aβ species are determined by ELISA. Panel D summarizes results from 3 correlated enzyme activity and ELISA tests. BACE1 activity and Aβ levels increase in parallel in 5XFAD cortical extracts age-dependently, and are higher relative to non-transgenics counterparts.

NIH-PA Author Manuscript
NIH-PA Author Manuscript
NIH-PA Author Manuscript

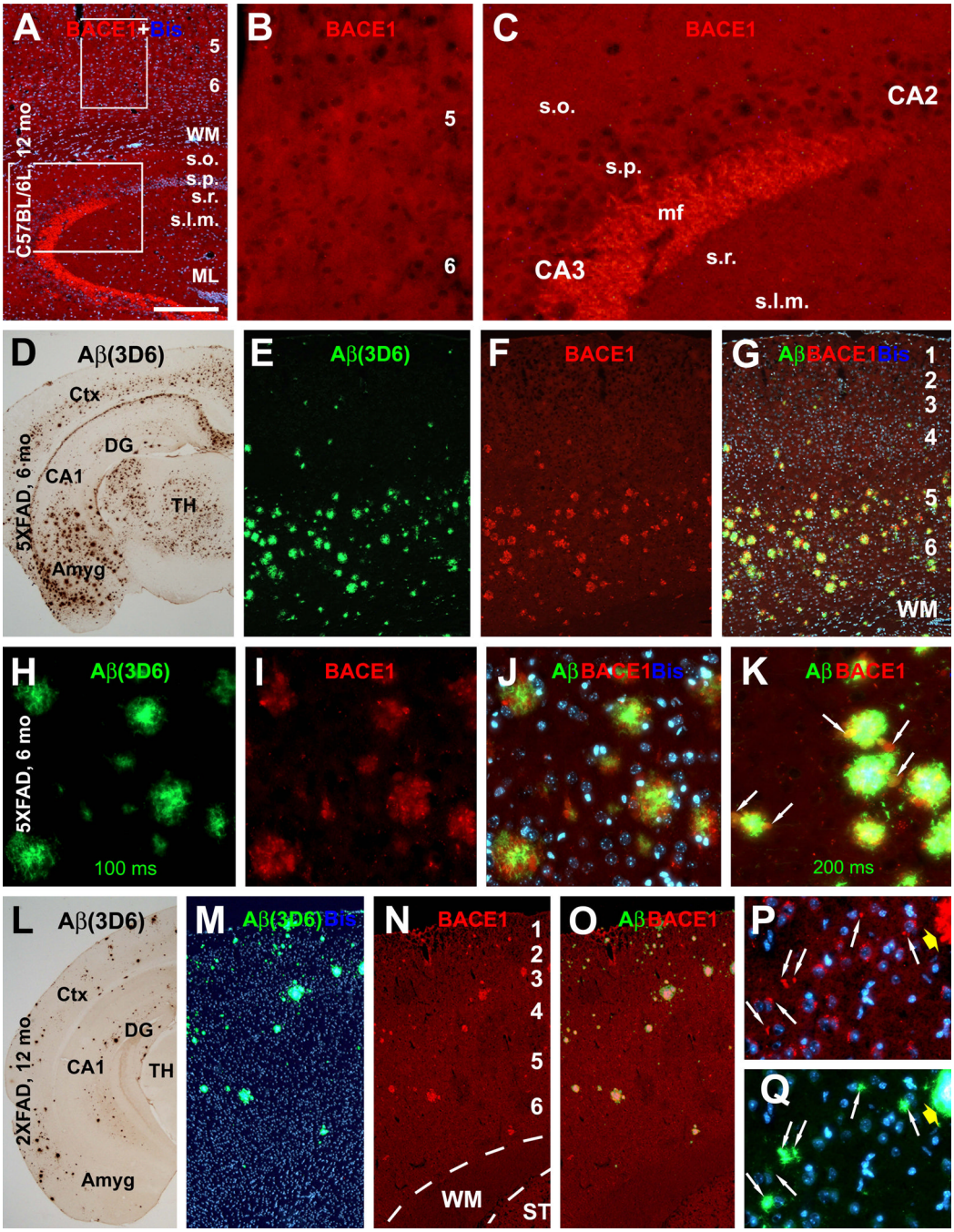

Fig. 3.

Selective BACE1 immunoreactivity (ir) in 5XFAD (D–K) and 2XFAD (L–Q) mouse brains around compact-like plaques. In batch-processed sections from a 12 month-old C57BL/6L mouse, BACE1 immunofluorescence appears as weak, background-like, reactivity in the cortex and hippocampus except for a heavy labeling at mossy fiber terminals (A–C). At low magnification, BACE1-ir occurs around virtually all plaque profiles visualized by monoclonal Aβ antibody 3D6 over the cortex in a 6 month-old 5XFAD (D–G) and a 12 month-old 2XFAD (L–O) mice. Shorter exposure (200 ms) for 3D6-ir displays compact plaques in star-fish appearance, with heaviest labeling localized to the plaque center surrounded by BACE1 labeled elements (H–J). With a slightly longer exposure (200 ms), 3D6-ir appears to extend beyond

NIH-PA Author Manuscript

NIH-PA Author Manuscript

NIH-PA Author Manuscript

BACE1 labeled profiles around individual plaques but occur inside BACE1 labeled profiles (K, arrows). Panels P and Q show small perisomatic elements (indicated by arrows) labeled for BACE1 (P) and 3D6 (Q) together with bisbenzimide counterstain (blue), in addition to a large plaque on the top-right edge of the images (pointed by fat yellow arrows). These small BACE1/Aβ immunoreactive profiles will be further addressed in detail. Amyg: amygdala, DG: dentate gyrus, s.o.: stratum oriens, s.p.: stratum pyramidale; s.r.: stratum radiatum, s.l.m.: stratum lacunosum-moleculare. Scale bar=500 μm in A, equal to 1 mm in D and L, 250 μm in E–G, M–O; and 100 μm in B, C, H–K, P, Q.

NIH-PA Author Manuscript
NIH-PA Author Manuscript
NIH-PA Author Manuscript

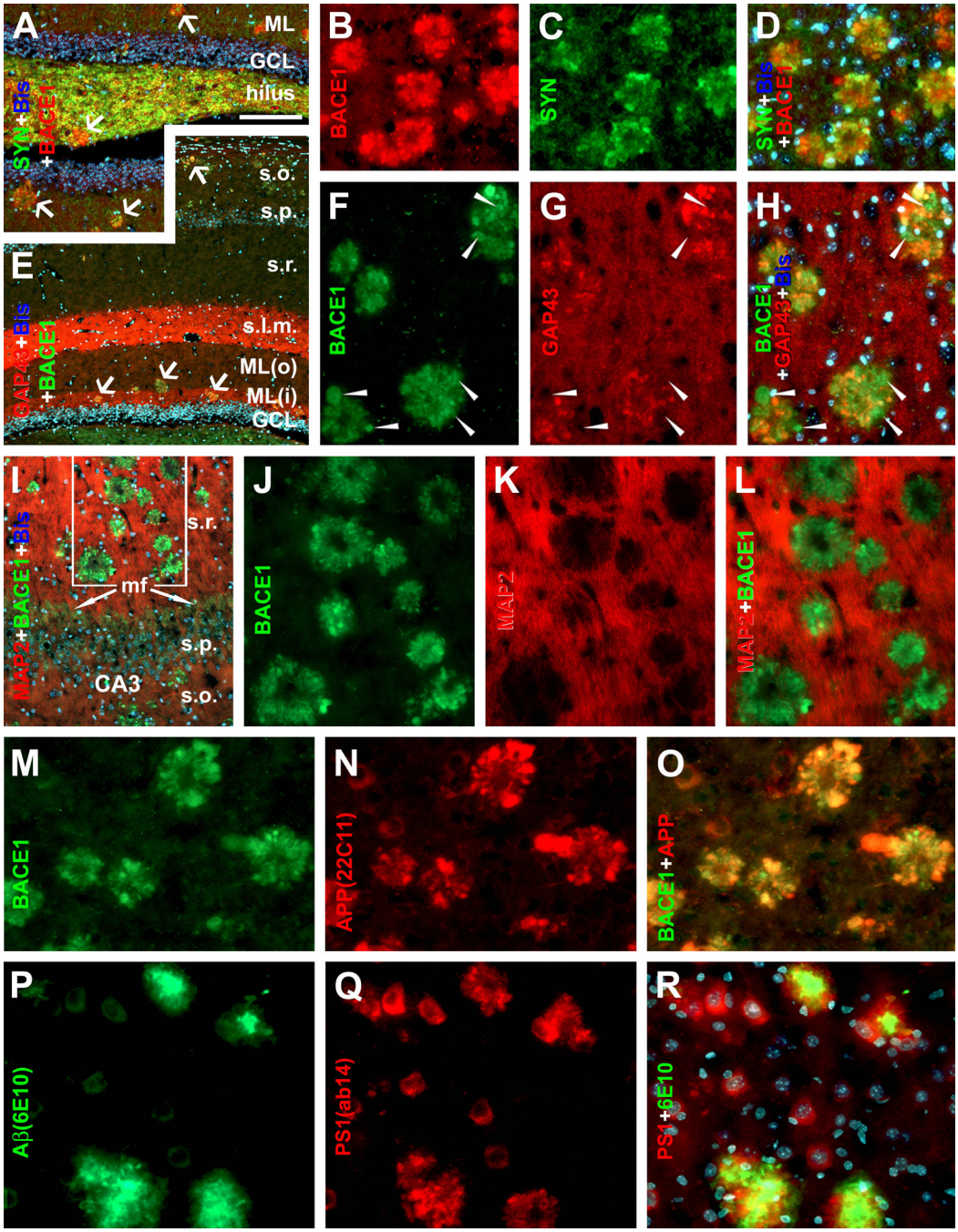

Fig. 4.

Localization of amyloidogenic proteins to axonal neurites around compact plaques in 5XFAD (8 month-old) mouse cortex and hippocampus. Panels A–D show virtually a complete colocalization of BACE1 with synaptophysin (SYN) in the dentate gyrus (A) and cortex (B–D). Panels E–H illustrate BACE1 colocalization with growth associated protein-43 (GAP43) in the hippocampal formation (E) and cortex (F–H). Some BACE1-contaning swollen terminals express low GAP-43 (arrowheads). BACE1 labeling does not colocalize with microtubule associated protein-2 (MAP2) (I–L). BACE1 labeled neurites also co-express APP (M–O) and possibly presenilin-1 (PS1) (P–R). Note that the monoclonal antibody 6E10 labels

extracellular Aβ deposits but also neuronal somata (P). Scale bar=250 μm in A applying to E, equal to 100 μm in I, 50 μm for remaining panels.

NIH-PA Author Manuscript
NIH-PA Author Manuscript
NIH-PA Author Manuscript

NIH-PA Author Manuscript
NIH-PA Author Manuscript
NIH-PA Author Manuscript

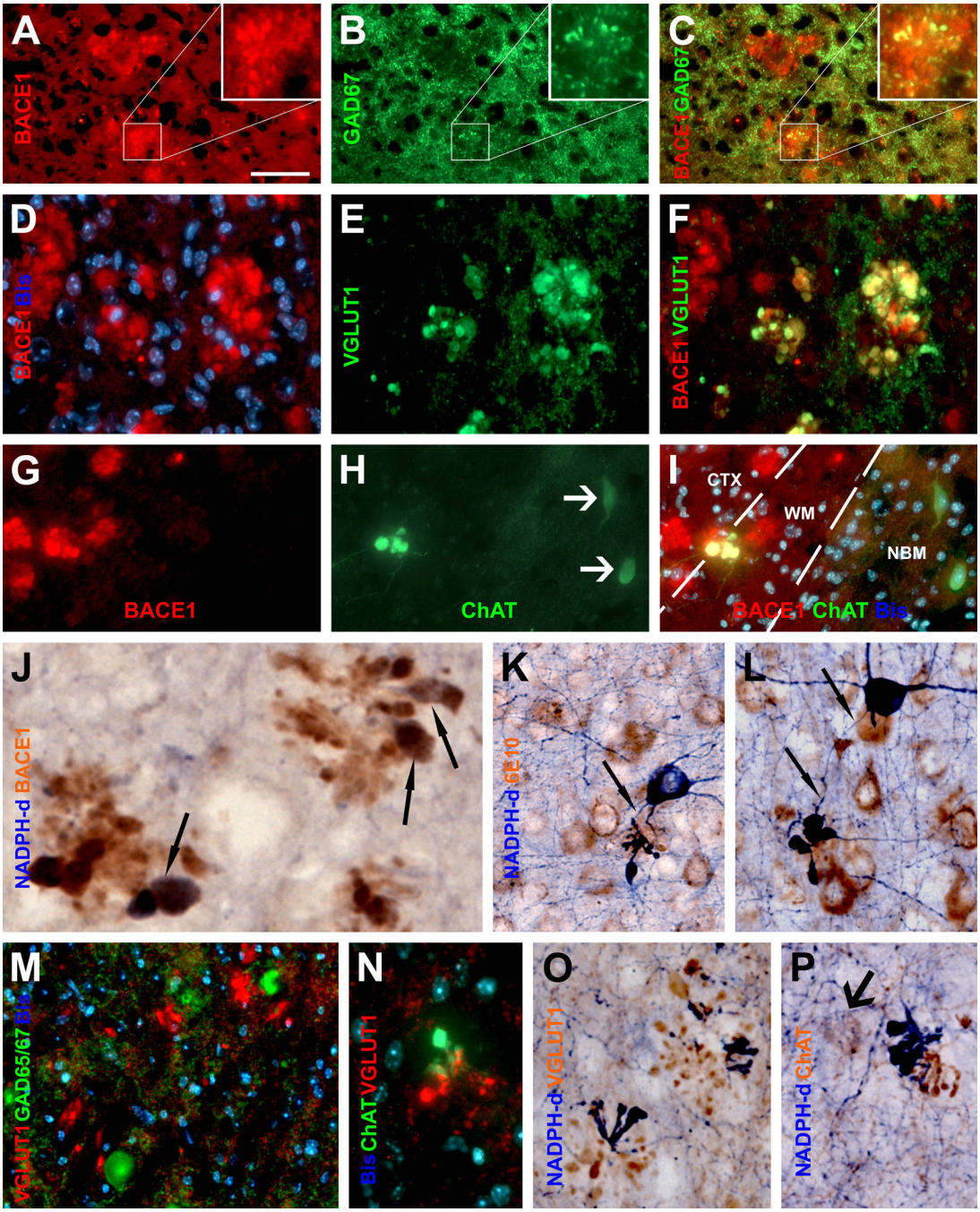

Fig. 5.

BACE1 localization to axonal dystrophic neurites in 5XFAD mouse forebrain. Subsets of BACE1 labeled dystrophic neurites coexpress glutamic acid decarboxylase-67 (GAD67) (A–C), vesicular glutamate transporter-1 (VGLUT1) (D-F), choline acetyltransferase (ChAT) (G–I). Panel J illustrates coexistence of BACE1-ir and β-nicotinamide adenine dinucleotide phosphate-diaphorase (NADPH-d) reactivity in dystrophic neurites (arrows) following a shorter histochemical reaction (15 minutes). Panels K and L show examples of dystrophic axons deriving from NADPH-d positive neurons (45 minutes reaction). Dystrophic neurites around the same plaque may express different neurotransmitter markers as indicated (M–P). NBM: nucleus basalis of Meynert. Arrows in (H, Q) point to cholinergic neuronal somata.

Scale bar=50 μm in A, applying to B–I, M, N; equal to 25 μm in K, L, O, P; and 12.5 μm in J.

NIH-PA Author Manuscript
NIH-PA Author Manuscript
NIH-PA Author Manuscript

NIH-PA Author Manuscript
NIH-PA Author Manuscript
NIH-PA Author Manuscript

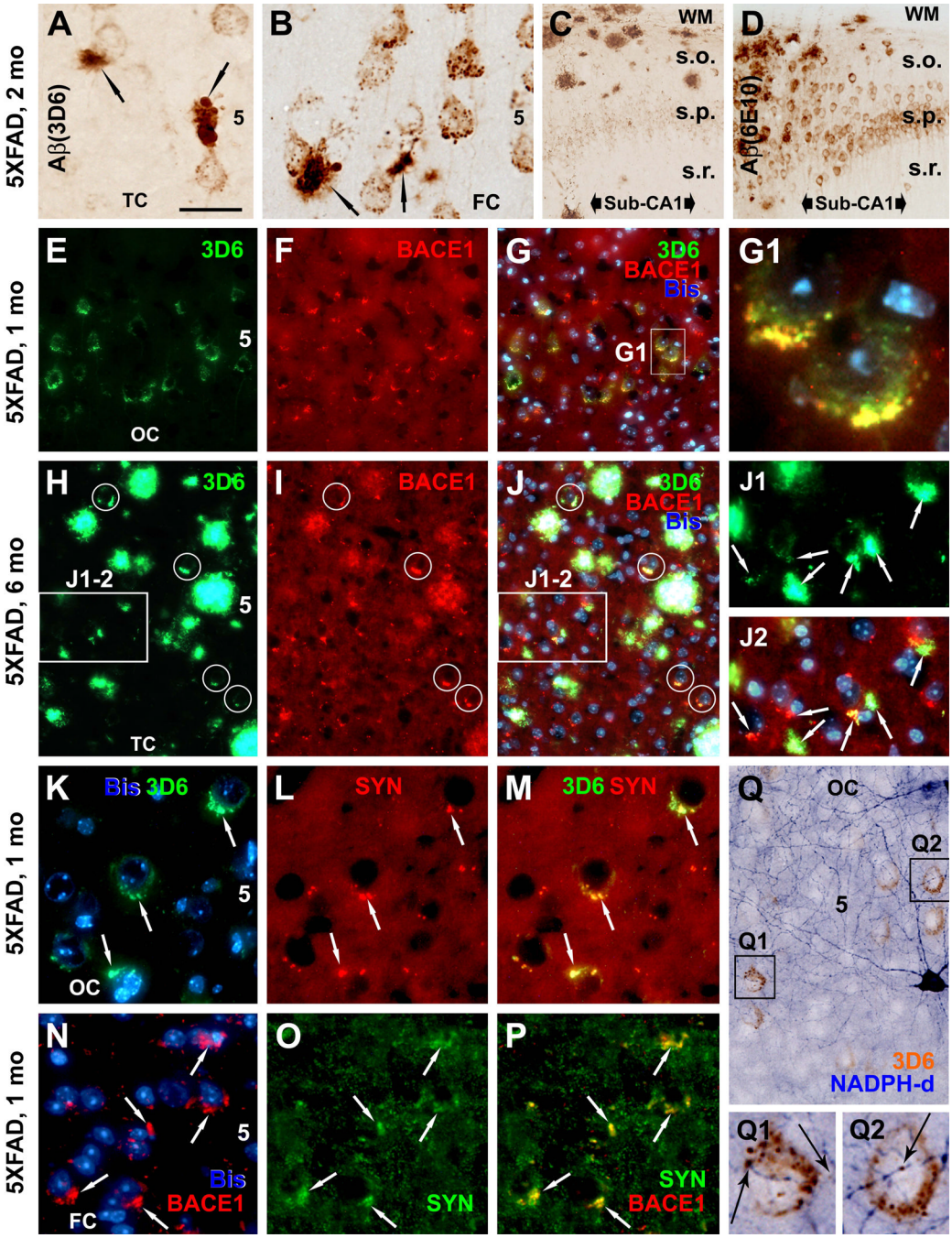

Fig. 6.

Occurrence of BACE1 and Aβ labelings at perisomatic axon terminals in 5XFAD mice before and after plaque onset at indicated ages. In a 2 month-old animal (A–D), 3D6-ir occurs over and/or around the perikarya of large layer V (A, B) and CA1 (C) pyramidal neurons as small granules, with varying densities from cell to cell. Small clusters of swollen neurites appear in layer V commonly next to pyramidal perikarya and are associated with local extracellular Aβ reactivity (A, B, arrows). Note that 3D6 and 6E10 both label extracellular Aβ deposits, whereas 6E10-ir, but not 3D6, also occurs in the cytoplasm of pyramidal neurons (D). In a 1 month-old mouse, BACE1 and 3D6 colocalization occurs selectively around a subset of layer V pyramidal neurons (E–G), with labeled elements appearing granule-like at high

NIH-PA Author Manuscript

NIH-PA Author Manuscript

NIH-PA Author Manuscript

magnification (G1). Panels H–J2 show a trend of evolution of BACE1/3D6 labeled perisomatic elements into "mini-plaques" consisted of small clusters of swollen neurites surrounded by local extracellular Aβ reactivity in 6 month-old mouse cortex. Several established compact plaques are present in the same field, which exhibit very bright 3D6 immunofluorescence. Panels K to M show colocalization of perisomatic 3D6-ir with synaptophysin (rabbit anti-SYN) around large layer V perikarya at 1 month of age. Similarly, BACE1 and synaptophysin (mouse anti-SYN) labelings colocalize at these perisomatic terminals in pre-plaque cortex (N–P). 3D6-ir also overlap locally at fine NADPH-d processes around or away from pyramidal perikarya (Q–Q2). OC: occipital cortex; TC: temporal cortex; FC: frontal cortex; Sub: subiculum. Scale bar=50 μm in A applying to K–M, J1–2 and N–O; equal to 200 μm for C, D; 100 μm for E–G, H–J and Q; and 12.5 μm for G1, Q1–2.

NIH-PA Author Manuscript

NIH-PA Author Manuscript

NIH-PA Author Manuscript

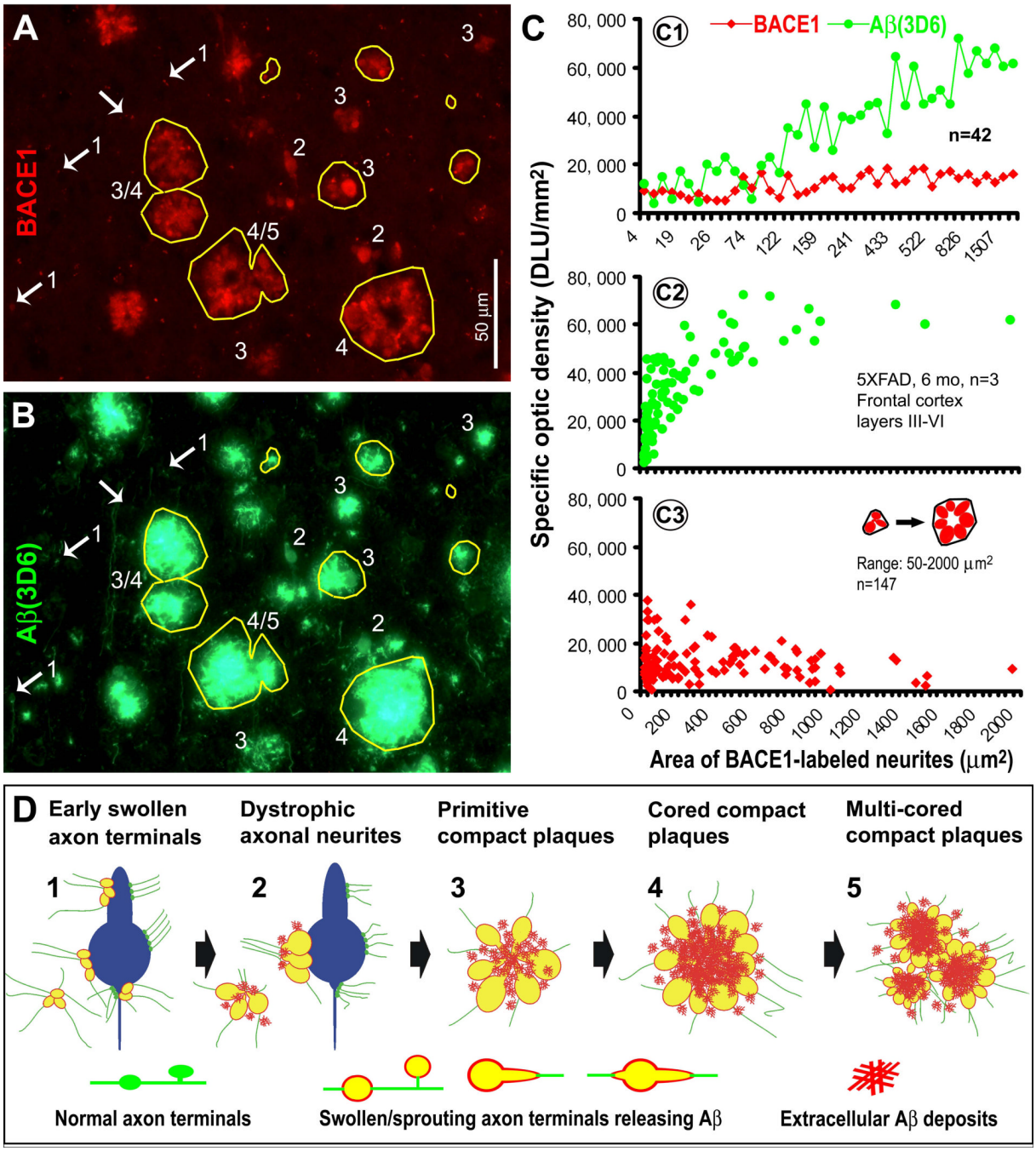

Fig. 7.

Densitometry and schematic drawing depicting a hypothesis that the onset and evolution of neuritic plaque may relate to a progressive axonal pathology inherent with intra-axonal Aβ genesis and local extracellular (extra-axonal) deposition. Panels A and B illustrate a method quantifying the areal sizes of, and BACE1/3D6-ir associated with, individual clusters of swollen/dystrophic neurites. Yellow cycles show examples for sampling the same set of profiles in BACE1 and 3D6 immunofluorescent images. Panel C1 plots data from 3 different microscopic fields (in the same section from a 6 month-old 5XFAD animal) showing relative specific densities of BACE1/3D6-ir among 42 clusters. BACE1-ir appears comparable among these clusters, whereas 3D6-ir appears to increase as clusters become >50–100 µm^2. Panels

NIH-PA Author Manuscript

NIH-PA Author Manuscript

NIH-PA Author Manuscript

C2 and C3 show trends of 3D6/BACE1-ir as a function of cluster size among ~150 profiles with areal sizes ≥ 50 μm^2 (data were from 15 high power fields from 3 animals, with 489 clusters quantified in total). 3D6-ir increases rapidly as the clusters enlarge from 50–1000 μm^2 (C2), whereas BACE1-ir maintains relatively stable (with a trend of decline in clusters larger than 1000 μm^2) (C3). Based on the above data and our anatomical studies, a hypothesis for neuritic plaque onset and evolution is illustrated schematically (D). Thus, Aβ rise at presynaptic terminals and/or axonal processes, mediated by BACE1 elevation at least in part, may consist of the first step of plaque-forming process. Axonal pathology manifests as continuous swelling and sprouting, resulting in the formation of dystrophic neurites. Meanwhile, the diseased axons produce and release Aβ into surrounding extracellular space. At certain stage, Aβ deposits begin to accumulate at the center inside the growing neuritic cluster (core-formation) because secreted Aβ from all or the majority of these neurites can reach this site (an overlapping zone). Cored Aβ deposits may stimulate or force neuritic outgrowth preferentially towards the periphery, resulting in a rosette-like neuritic distribution pattern. Multi-cored plaques may form as axonal pathology and amyloidogenesis continue, or as neighboring plaques merge. Arab numbers and arrows in panels A, B and C point to representative profiles at artificially-defined corresponding stages of plaque development, including those potentially at transitional states (e.g., profiles marked with "3/4" and "4/5" in A, B).

NIH-PA Author Manuscript
NIH-PA Author Manuscript
NIH-PA Author Manuscript

Table 1

Primary antibodies used in the present study

Antibody	Source	Product #	Dilution
mouse anti-Aβ1–5, 3D6	Elan	Lot#1132	1:3000
mouse anti-Aβ17–26, 4G8	Signet	39240	1:2000
biotinylated mouse anti-Aβ17–26, 4G8	Signet	9240–02	1:4000
mouse anti-Aβ1–16, 6E10	Signet	39320	1:4000
rabbit anti-Aβ35–40	H. Mori	Ter-40	1:3000
rabbit anti-Aβ38–42	H. Mori	Ter-42	1:3000
mouse anti-amyloid precursor protein, 22C11	Millipore	MAB348	1:1000
rabbit anti-BACE1 (a.a. 46–163)	H. Cai	anti-BACE1α	1:2000
mouse anti-calbindin	Sigma	C9848	1:4000
goat anti-choline acetyltransferase	Millipore	AB1447	1:1000
rabbit anti-glutamic acid decarboxylase (GAD) 65/67	Millipore	AB1511	1:2000
mouse anti-GAD67	Millipore	MAB5406	1:4000
mouse anti-growth- associated protein	Sigma	G9264	1:4000
rabbit anti-glial fibrillary acidic protein	Sigma	G9269	1:4000
mouse anti-microtubule associated protein-2	Sigma	M9942	1:1000
rabbit anti-presenilin-1	S. Gandy	ab14	1:500
mouse anti-parvalbumin	Sigma	P3088	1:4000
mouse anti-synaptophysin	Millipore	MAB329	1:4000
rabbit anti-synaptophysin	Epitomics	1485–1	1:1000
rabbit anti-β-tubulin-III	Sigma	T2200	1:10000
mouse anti-tyrosine hydroxylase	Sigma	T2928	1:4000
mouse anti-vesicular glutamate transporter-1	Millipore	MAB5502	1:2000